

6

6

# Control over emissivity of zero-static-power thermal emitters based on phase-changing material GST

K. Kim<sup>1</sup>, D. Kim<sup>1</sup>, Y. Baek<sup>2</sup>, J. Cho<sup>1</sup>, A. Kim<sup>1</sup>, H. Yoon<sup>2</sup>

1, 2

<sup>1</sup>KAIST

6 6

6

6

6B10027, 6

6

<sup>2</sup>KAIST

6B10027

6B10027, 6

E-mail

# 1. Infrared property of amorphous and crystalline GST

Figure 1 shows the infrared properties of amorphous and crystalline GST on Si substrate, measured from 360 nm to 1600 nm.

The wavelength range is from 360 nm to 1600 nm.

The figure shows the reflectivity and transmissivity of the GST films.

The reflectivity and transmissivity are plotted against the wavelength.

The figure is divided into two parts, (a) and (b).

Part (a) shows the reflectivity and transmissivity of the GST films on Si substrate.

Part (b) shows the refractive index and extinction coefficient of the GST films.

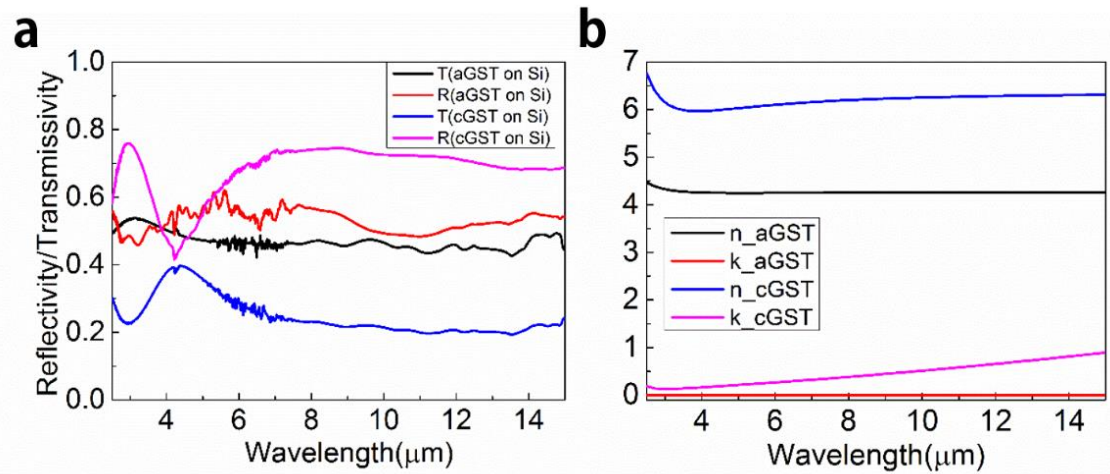


Fig. 1. (a) Reflectivity and transmissivity of GST on Si substrate.

(b) Refractive index and extinction coefficient of GST on Si substrate.

Figure 1

## 2. Angular-dependent absorption of the cGST-Au sample

Figure 2 shows the angular-dependent absorption of the cGST-Au sample. The absorption spectra were measured at different incident angles (0°, 20°, 40°, and 60°) in the wavelength range of 6-15 μm. The absorption spectra show a resonance peak around 9.5 μm. The absorption intensity increases with the incident angle, and the resonance peak shifts to shorter wavelengths as the angle increases. The simulation results (a) and experimental results (b) are compared, showing a good agreement between the two.

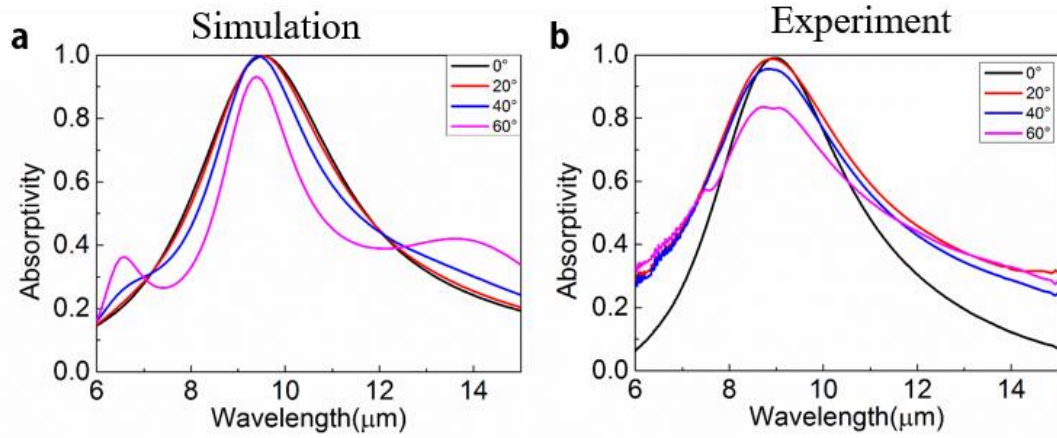


Figure 2. Angular-dependent absorption of the cGST-Au sample. (a) Simulation results and (b) experimental results. The absorption spectra were measured at different incident angles (0°, 20°, 40°, and 60°) in the wavelength range of 6-15 μm. The absorption intensity increases with the incident angle, and the resonance peak shifts to shorter wavelengths as the angle increases. The simulation results (a) and experimental results (b) are compared, showing a good agreement between the two.

### 3. The role of the metal film in the GST-Au absorber/emitter

The figure shows the absorptivity spectra for four different structures. The x-axis represents Wavelength ( $\mu\text{m}$ ) from 6 to 15, and the y-axis represents Absorptivity from 0.0 to 1.0. The structures are:

- (1) 450 nm GST-PEC: Black curve, peak absorptivity ~0.95 at 11.5  $\mu\text{m}$ .
- (2) 450 nm GST-Au: Red curve, peak absorptivity ~0.95 at 11.5  $\mu\text{m}$ .
- (3) 900 nm GST-Air: Blue curve, peak absorptivity ~0.55 at 11.5  $\mu\text{m}$ .
- (4) 900 nm GST-1.5: Magenta curve, peak absorptivity ~0.45 at 11.5  $\mu\text{m}$ .

The legend in the figure identifies the curves as:

- 450 cGST-PEC (Black)
- 450 cGST-Au (Red)
- 900 cGST-Air (Blue)
- 900 cGST-1.5 (Magenta)

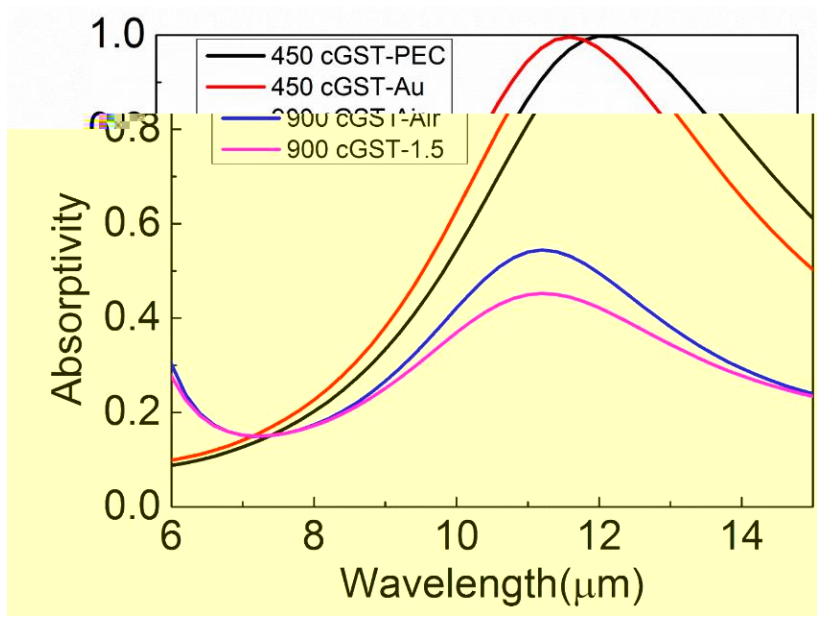


Fig. 8. Absorptivity spectra

Figure 1.5.

## Resonance

When the system is driven

at a frequency  $\omega$

## Steady-State Solution

Let  $x(t) = A e^{j\omega t}$  and  $\dot{x}(t) = j\omega A e^{j\omega t}$

Then  $|s_i|^2$  is

the real part of  $\frac{1}{j\omega - \gamma_1 - \gamma_2}$

$\omega_0$ , the imaginary part is

the imaginary part of  $\frac{1}{j\omega - \gamma_1 - \gamma_2}$ :

$$\frac{d}{dt} a = (j\omega_0 - \gamma_i - \gamma_1 - \gamma_2)a - j\sqrt{2\gamma_1} s_i \quad (S)$$

If  $A(\omega)$  is the amplitude and  $\theta(\omega)$  is the phase

## Amplitude

$$A = \frac{4\gamma_i\gamma_1}{(\omega - \omega_0)^2 + (\gamma_i + \gamma_1 + \gamma_2)} \quad (S2)$$

For  $\gamma_1 = \gamma_2$ , the maximum is 50% at

$\omega = \omega_0$ . The phase is  $\theta = -\frac{\pi}{2}$  at  $\omega = \omega_0$ , 100% at

$\omega = \omega_0 + \frac{\gamma_i + \gamma_1 + \gamma_2}{2}$  and  $\theta = 0$  at  $\omega = \omega_0 - \frac{\gamma_i + \gamma_1 + \gamma_2}{2}$ .

The phase is  $\theta = -\frac{\pi}{4}$  at  $\omega = \omega_0 + \frac{\gamma_i + \gamma_1 + \gamma_2}{4}$

## Quality Factor

is defined as

$Q = \frac{\omega_0}{\gamma_i + \gamma_1 + \gamma_2}$  . For  $\gamma_1 = \gamma_2$

the quality factor is  $Q = \frac{\omega_0}{2\gamma_i}$  . *Opt. Express*. 2010; **18**: 8367-8382.

See also [http://www.riken.ac.jp](#)

For a more detailed analysis, see *IEEE J. Quantum Electron.* 1999; **35**: 1322-1331.

#### 4. Emission spectra and emissivity differences of aGST-Au and cGST-Au emitters

Figure 4 shows the emission spectra and emissivity differences of aGST-Au and cGST-Au emitters. The figure is divided into two parts, (a) and (b). Part (a) shows the emitted power (a.u.) versus wavelength (μm) for four different emitters: Black soot (purple), 360nm (black), 450nm (blue), and 540nm (green). Part (b) shows the emissivity difference versus wavelength (μm) for the same four emitters. The emissivity difference is defined as the difference in emissivity between the two emitters at a given wavelength.

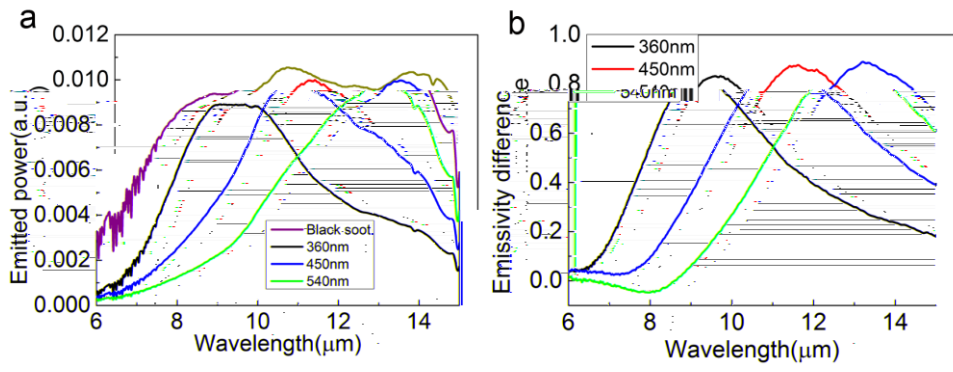
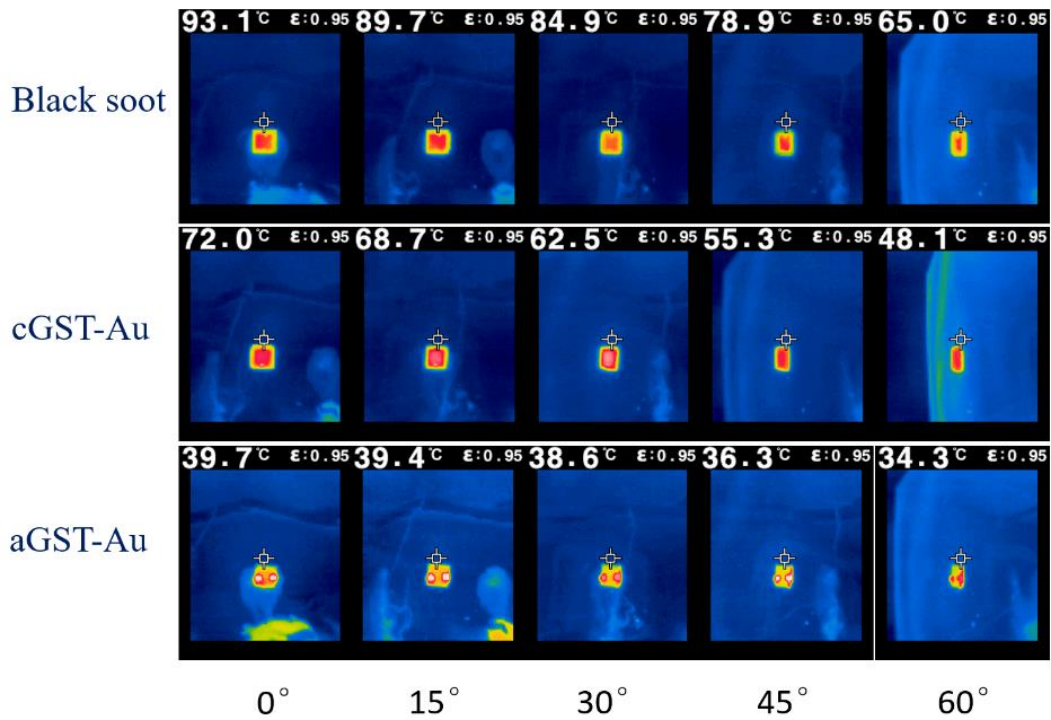


Fig. 4. (a) Emission spectra of aGST-Au and cGST-Au emitters at 360 nm, 450 nm, and 540 nm. (b) Emissivity differences of aGST-Au and cGST-Au emitters at 360 nm, 450 nm, and 540 nm.

## 5. Angular-dependent infrared photographs of the black soot and the GST-Au emitter

The infrared photographs were taken at a distance of 540 mm from the emitter. The temperature of the emitter was maintained at 100°C. The emissivity of the emitter was 0.95. The photographs were taken at angles of 0°, 15°, 30°, 45°, and 60°. The photographs show the distribution of the infrared radiation emitted by the black soot and the GST-Au emitter. The black soot emitter shows a more uniform distribution of radiation, while the GST-Au emitter shows a more directional distribution.



The photographs were taken at angles of 0°, 15°, 30°, 45°, and 60°.

## 6. Tunable thermal emission of the GST-Au emitter by controlling the annealing temperature

Figure 6. (a)  $\text{Re}(\tilde{\epsilon})$  and (b)  $\text{Im}(\tilde{\epsilon})$  of the GST-Au emitter.

Figure 6. (a)  $\text{Re}(\tilde{\epsilon})$  and (b)  $\text{Im}(\tilde{\epsilon})$  of the GST-Au emitter.

Figure 6. (a)  $\text{Re}(\tilde{\epsilon})$  and (b)  $\text{Im}(\tilde{\epsilon})$  of the GST-Au emitter.

Figure 6. (a)  $\text{Re}(\tilde{\epsilon})$  and (b)  $\text{Im}(\tilde{\epsilon})$  of the GST-Au emitter.

Figure 6. (a)  $\text{Re}(\tilde{\epsilon})$  and (b)  $\text{Im}(\tilde{\epsilon})$  of the GST-Au emitter.

Figure 6. (a)  $\text{Re}(\tilde{\epsilon})$  and (b)  $\text{Im}(\tilde{\epsilon})$  of the GST-Au emitter.

Figure 6.

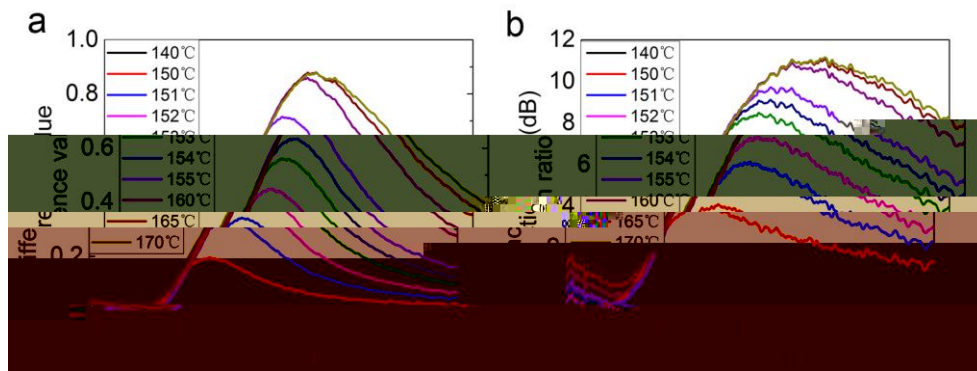


Figure 6. (a)  $\text{Re}(\tilde{\epsilon})$  and (b)  $\text{Im}(\tilde{\epsilon})$  of the GST-Au emitter.

Figure 6. (a)  $\text{Re}(\tilde{\epsilon})$  and (b)  $\text{Im}(\tilde{\epsilon})$  of the GST-Au emitter.

Figure 6.

7. Controlling the intermediate GST by both the annealing temperature and the annealing time.

Figure 7. Absorbance spectra of GST film annealed at 150°C, 160°C, 170°C, and 180°C for 500 s. The inset shows the absorbance spectra of GST film annealed at 150°C for 0 s, 50 s, and 100 s. The inset shows that the absorbance of GST film increases with annealing time at 150°C.

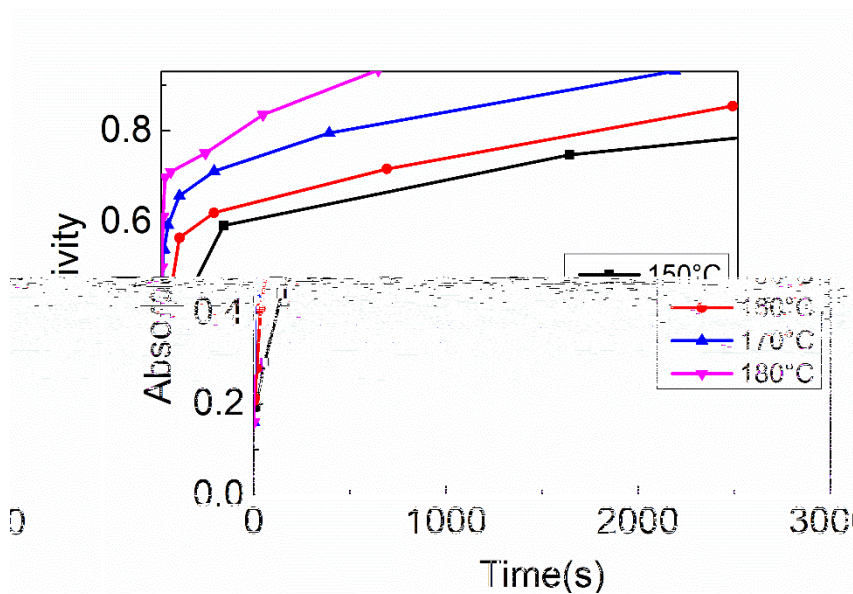


Figure 7. Absorbance spectra of GST film annealed at 150°C, 160°C, 170°C, and 180°C for 500 s.

Figure 7. Absorbance spectra of GST film annealed at 150°C, 160°C, 170°C, and 180°C for 500 s.

## 8. Reamorphization of cGST

Figure 6c

Figure 6b

Figure 6a

Figure 6d

Figure 6e

-m -k

Figure 6f

Figure 6g

Figure 6h

Figure 6i

-m -k

Figure 6j

Figure 6k

Figure 6l

Figure 6m

Figure 6n

Figure 6o

Figure 6p

Figure 6q

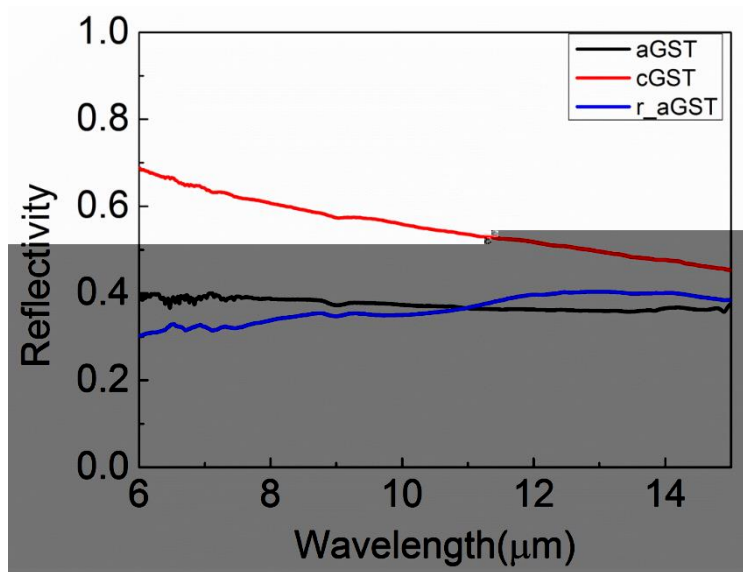


Figure 8. Reamorphization of cGST

500-m -k

## 9. Dual-band absorption and emission of the samples.

Fig. 9

(a)

(b)

(c)

Fig. 9

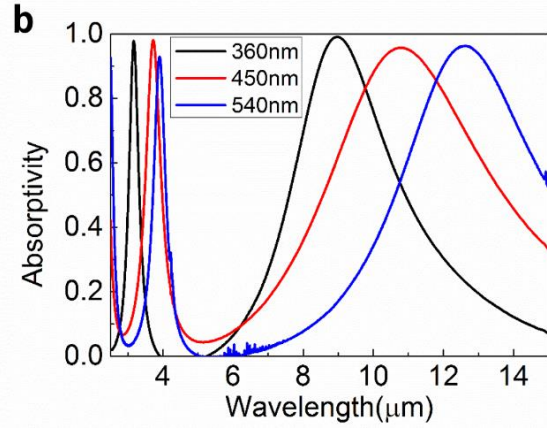
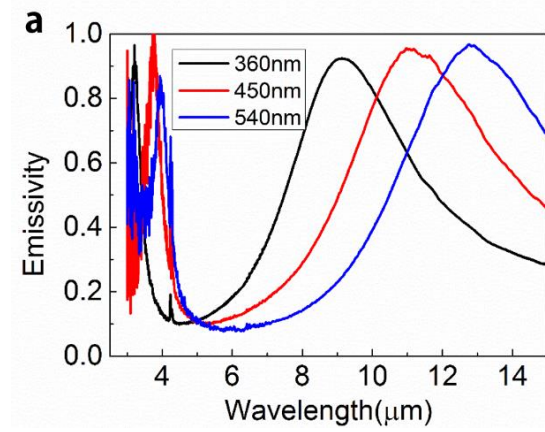


Fig. 9

Fig. 9

Fig. 9

Fig. 9